Synthesis and Characterization of Thick Porous Bismuth Oxide Films for Resistive Gas Sensing Applications

R. R. Attarde
Department of Physics, M. J. College, Jalgaon (MS) India.

Abstract : Nanostructured MnO_2 powders were synthesized by hydrolysis of AR grade manganese chloride in aqueous-alcohol solution with bismuth chloride (dopant in the proportion 1, 3, 5 and 7 wt %) to get fine powder. Thick films of Bi_2O_3-doped MnO_2 powders were prepared by screen printing technique. The structural properties of these films were studied by X-ray diffraction technique. The XRD spectrum revels that the films are polycrystalline in nature and monoclinic in structure. The average grain size was determined using Scherrer's formula and was estimated to be of 396 nm. It was also observed that, the amorphous nature decreases (i. e. crystalline nature increases) with the percentage of doping with bismuth oxide. The SEM analysis, it is clear that with the increase of doping concentration, there is a change in the surface texture of the films. Larger the doping concentration, larger would be the amount of Bi_2O_3 dispersed on the surface, and smaller would be the chances of reaching the gas to base material. The I-V characteristics of the pure and Bi_2O_3 doped MnO_2 films at room temperature and at high temperature shows that the contacts fabricated on the films were ohmic in nature and the p-n junctions were randomly distributed on the surface of the film. The conductivity values of all samples were larger at room temperature than at higher temperature. It may be due to air humidity associated with the films at room temperature. The increase in conductivity with increasing temperature (above 50^0C) could be attributed to negative temperature coefficient and semiconducting nature of the Bi_2O_3 activated MnO_2 samples. The Bi_2O_3 activated films showed very high electrical resistance of the order of 10^5 Ω in air.

Keywords: Bi_2O_3-doped MnO_2, XRD, SEM, conductivity.

I. INTRODUCTION

The semi-conductive properties of metal oxides represent the basis for their use as resistive gas sensors, since the number of free charge carriers within the metal oxide and thus its electrical conductivity reversibly depends on the interactions with the ambient gas atmosphere. Mixed metal oxides offer the advantage of comparably simple production and broad availability, and at the same time provide the potential for a sufficiently low base resistance and an adequate durability in long-term operation. Their use is currently still restricted by the cross sensitivity of the known sensor materials. Lately mixed metal oxides, which combine the positive sensor properties of the pure components, are used for gas detection purposes [1 - 3]. However, with the help of classical synthesis methods of oxidic sensors such as sputtering, CVD (chemical vapour deposition), PLD (pulsed laser deposition), and MBE (molecular beam epitaxy) [4 - 6] only thin films can be produced.

Espinosa et al. studied the electrochemical properties of Bi_2O_3 mixing it with carbon powder in strongly alkaline solution [7]. They observed that a chemical reaction occurs between bismuth oxide and OH– ions, while the electrochemical reduction of BiO_2 is occurring at –0.8 V.

2. Experimental procedure

2.1 Synthesis of nanostructured MnO_2 powder

Nanostructured Bi_2O_3-doped MnO_2 powders was synthesized by hydrolysis of AR grade manganese chloride in aqueous-alcohol solution. An initial aqueous-alcohol solution was prepared from distilled water and propylene glycol in the ratio of 1:1. This solution was then mixed with aqueous solution of manganese chloride and bismuth chloride (dopant in the proportion 1, 3, 5 and 7 wt %) in the ratio such that the elemental concentration was 0.1M and the alcohol to water ratio was 1:1. The special arrangement was made to add drop wise aqueous ammonia (0.1ml / min.) with constant stirring till the optimal pH of solution becomes 8.3. After complete precipitation, the hydroxide was washed with distilled water until chloride ions were not detected by

$AgNO_3$ solution. Then the hydroxide in a glass beaker was placed in a microwave oven for 15 minutes with on-off cycles, periodically. The dried precipitate was ground by agate pestle-mortar and annealed in a muffle furnace at 600°C for 3h. The fine powders were calcined at 800^0C for 24 h, in air and re-ground, to ensure sufficiently fine particle size.

2.2 Thick film fabrication

Thick films of Bi_2O_3-doped MnO_2 powders were prepared using following procedure. The thixotropic pastes [8, 9] were formulated by mixing the resulting fine powders with a solution of ethyl cellulose (a temporary binder) in a mixture of organic solvents such as butyl cellulose, butyl carbitol acetate and turpineol. The ratio of inorganic to organic part was kept as 75:25 in formulating the pastes. The thixotropic pastes were screen printed on a glass substrate in desired patterns. The films prepared were fired at 500^0C for 24 h in ambient air.

3. Materials characterization

3.1 Structural properties (X-ray diffraction studies)

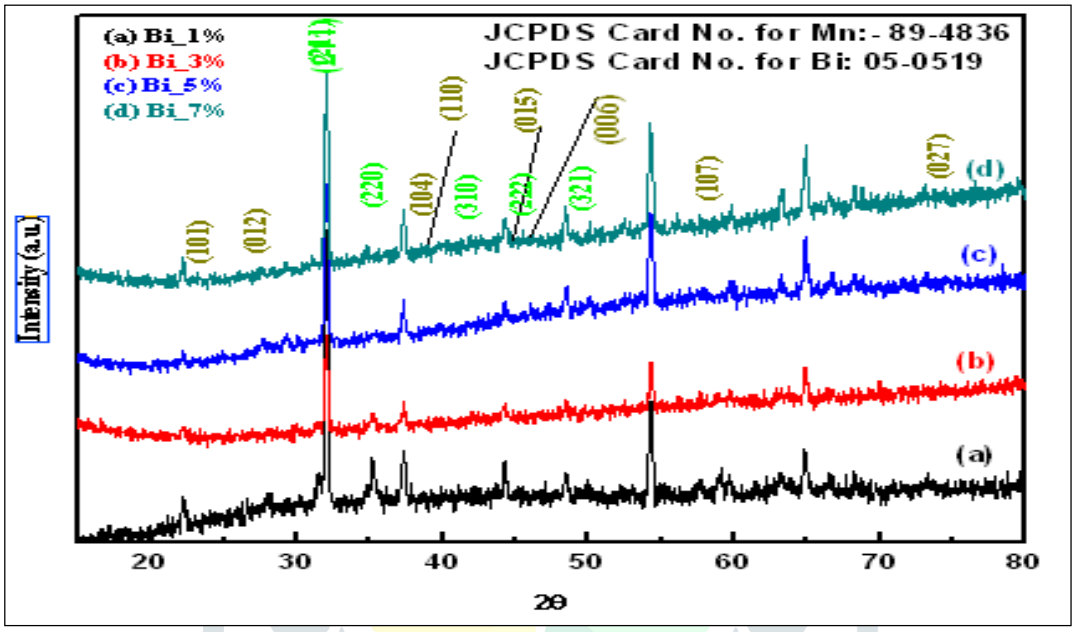

Fig. 1 XRD of pure and Bi_2O_3 - doped MnO_2 powders

X ray diffraction study of Bi_2O_3 doped MnO_2 thick films was carried out using BRUKER AXSD8 (Germany) advance model X ray diffraction with $CuK\alpha_1$ (λ=1.54056 Å) radiation in the 2θ range 20^0- 80^0. The scanning speed of the specimen was maintained 0.5^0 /min. Figure 1 shows the XRD pattern of Bi_2O_3 doped MnO_2 thick films. The 2θ peak observed at 22.23, 26.55, 32.052, 35.28, 37.33, 39.24, 42, 44.26, 46, 48.47, 54.29, 57.04 and 73 which correspond to the (101), (012), (211), (220), (104), (110), (310), (015), (222), (006), (321), (107) and (027) planes of reflections. The XRD spectrum revels that the films are polycrystalline in nature and monoclinic in structure. Figure depicts the XRD of surface activated MnO_2. The observed peaks are matching well with ASTM reported data of pure MnO_2 doped with Bi_2O_3. The material was observed to be nanocrystalline in nature. There are no prominent peaks of Bi_2O_3 associated in XRD pattern of MnO_2 due to smaller wt % of Bi_2O_3 in comparison with MnO_2. The lattice parameters were found to be a = 5.83, b = 8.14 and c = 7.48. The unit cell volume was evaluated as 326.92. (JCPDS data card no. for Mn – 89 – 4836 and Bi – 05 - 0519). The average grain size was determined using Scherrer's formula and was estimated to be of 396 nm.

Table 1: Percentage crystallinity and amorphous nature of as synthesized powders

Material	Doping (%)	Crystalline (%)	Amorphous (%)
Bi_2O_3 doped MnO_2	1	42.4	57.6
	3	45.6	54.4
	5	50.7	49.3
	7	58.6	41.4

It was also observed from XRD analysis that, the amorphous nature decreases (i. e. crystalline nature increases) with the percentage of doping with bismuth oxide (Table 1). This may be attributed to the fact that, on doping, cadmium reacts and makes tight binding with the manganese which would require more ultrasonic power to make the powder amorphous.

3.2. Micro structural analysis of Bi_2O_3 doped MnO_2

Fig. 2 (a - c) depicts the microstructure of Bi_2O_3 (1 wt %) doped MnO_2 film consisting of smaller grains of Bi_2O_3associated with the larger grains of MnO_2. The larger grains of MnO_2 occurred due to agglomeration of its smaller grains. The film consists of island like structure and grains with sizes ranging from 51.4 nm to 109 nm distributed non-uniformly. Fig. 2 (d -f) depicts the microstructure of Bi_2O_3 (3 wt %) doped MnO_2 film, consisting of number of particles of Bi-species distributed on the MnO_2 surface. Figure shows that a few grains of MnO_2 in the film are masked with a very thin layer of Bi-species. This film was observed to be the most sensitive film. The masking of the films increases with doping concentration. The entire masking of the films in sufficient proportion resists the gas to reach the active sites of the surface of the film. The grain sizes vary from 23.2 nm to 60.6 nm. Fig. 2 (g - i) depicts the microstructure of Bi_2O_3 (5 wt %) doped MnO_2 film smaller grains of Bi_2O_3 in association with MnO_2 as compared to that in Figs. 2 (d - f). The most of the grains of MnO_2 are covered with smaller grains of Bi_2O_3. The grains of MnO_2 are having cubical shape and size and oriented randomly. The films consist of voids and a wide range of grains with grain sizes ranging from 73.7 nm to 107 nm distributed non-uniformly. Fig. 2 (j - l) depicts the microstructure of Bi_2O_3 (7 wt %) doped MnO_2 film consisting of smaller grains of Bi_2O_3 in association with larger grains of MnO_2. The masking of the films increases with doping concentration. The entire masking of the films in sufficient proportion resists the gas to reach the active sites of the surface of the film. This would decrease the gas sensing performance of the films at higher doping concentration (i. e. > 5 %). It is clear from figures that with the increase of doping concentration, there is a change in the surface texture of the films. Larger the doping concentration, larger would be the amount of Bi_2O_3 dispersed on the surface, and smaller would be the chances of reaching the gas to base material. The doping concentration was, therefore, optimized to have optimum number of Bi_2O_3 misfits dispersed uniformly on the surface so as to contribute effective enhancement of gas sensing.

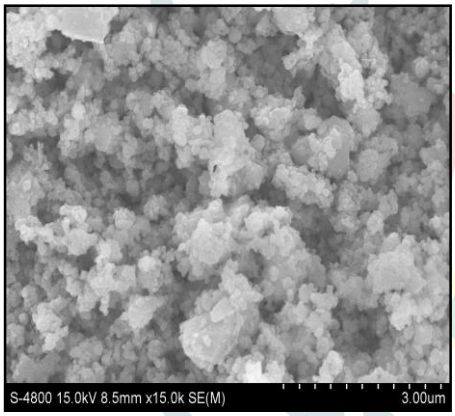

(a)

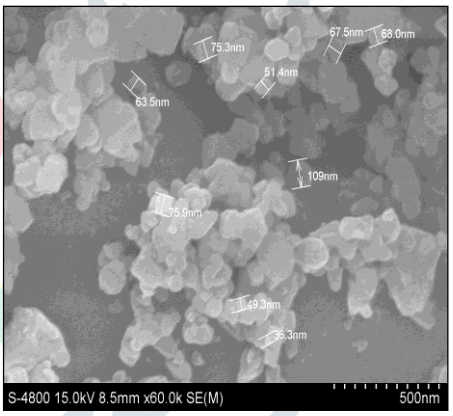

(b)

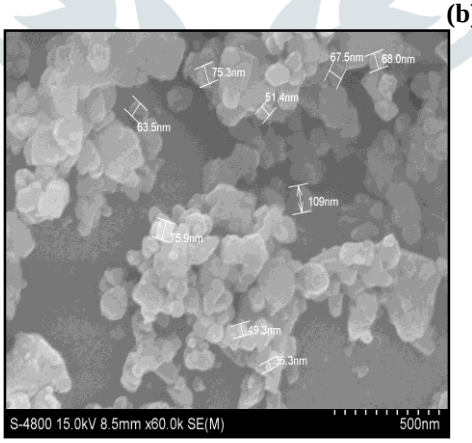

(c)

Fig. 2 (a-c): Micrograph of modified MnO_2 film (1 wt %)

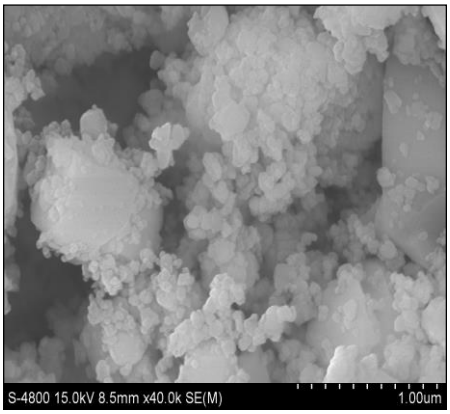

(d)

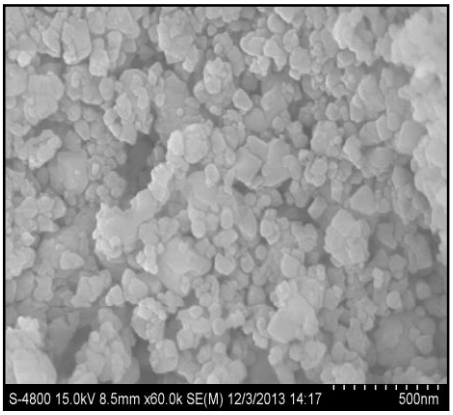

(e)

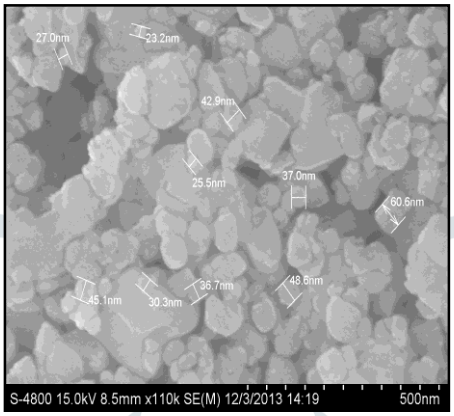

(f)

Fig. 2 (d-f): Micrograph of modified MnO_2 film (3 wt %)

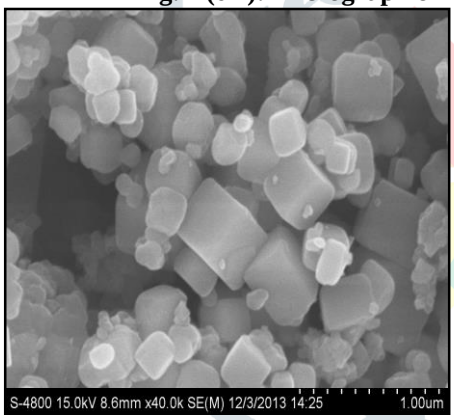

(g)

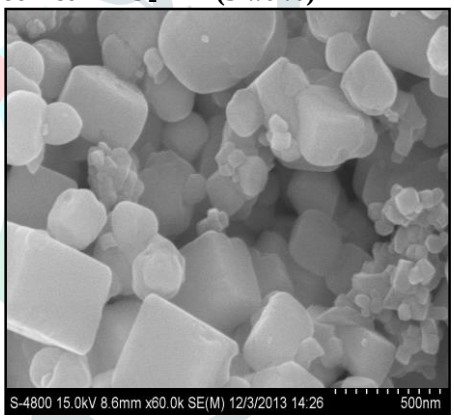

(h)

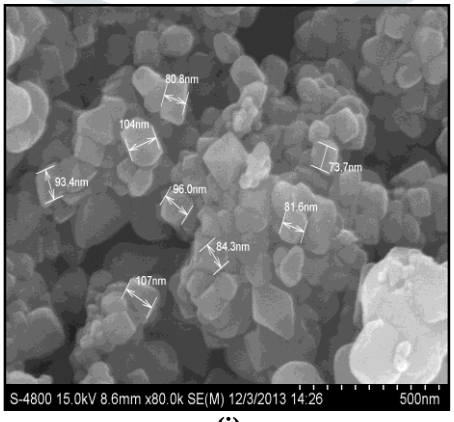

(i)

Fig. 2 (g-i): Micrograph of modified MnO_2 film (5 wt %)

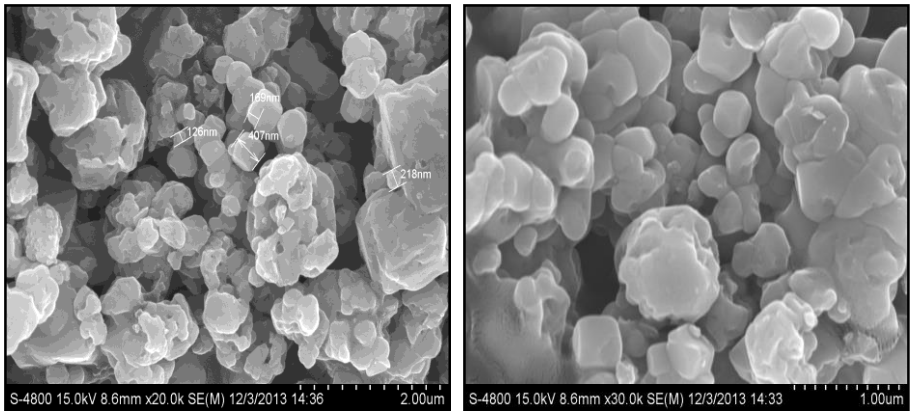

(j) **(k)**

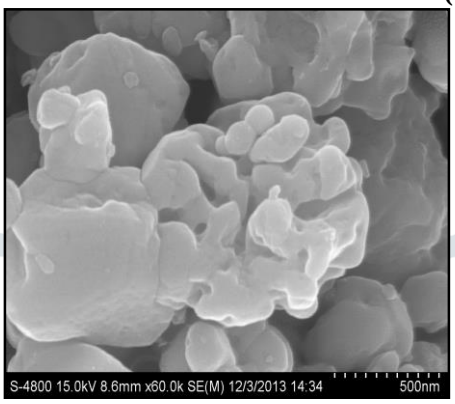

(l)

Fig. 2 (j-l): Micrograph of modified MnO_2 film (7 wt %)

3.3 I-V characteristics

Fig. 3 (a, b) represents I-V characteristics of the pure and Bi_2O_3 doped MnO_2 films at room temperature and at high temperature. It is clear from the symmetrical I-V characteristics that the contacts fabricated on the films were ohmic in nature and the p-n junctions were randomly distributed on the surface of the film. The material is therefore said to have resistive properties.

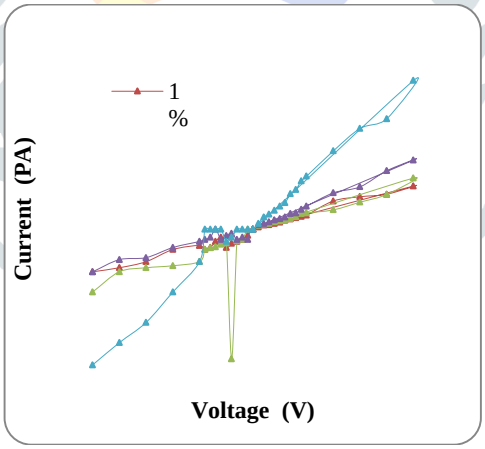

Fig. 3 (a) I-V characteristics of sensor (RT)

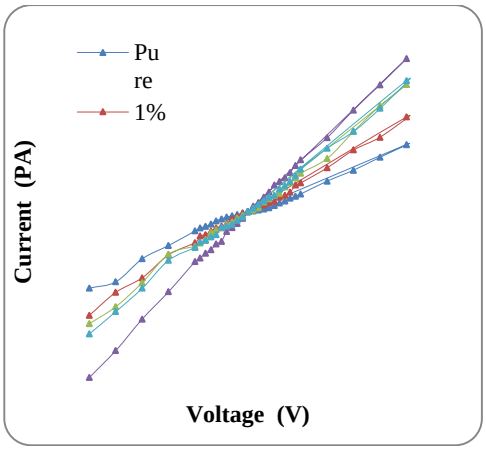

Fig. 3 (b) I-V characteristics of sensor (High Temperature)

3.4 Electrical conductivity

Fig. 4 shows the variation of conductivity with the reciprocal of operating temperature. The conductivities of all samples are decreasing with increase in operating temperature. The decrease in conductivity with increase in temperature could be attributed to negative temperature coefficient of resistance and semiconducting nature of the Bi_2O_3 modified MnO_2. It is observed that the electrical conductivities of the pure and Bi_2O_3 modified MnO_2 films are increasing gradually in the temperature ranges from 100^0C to 300^0C and increasing drastically linearly above 300^0C in air ambient. The conductivity of pure MnO_2 decreases slowly than the modified films, even at higher temperatures. Pure MnO_2 has only one kind of grains arranged uniformly. However, the modified films cause the formation of heterogeneous intergrain boundaries of Bi_2O_3-MnO_2 grains. The conductivity values of all samples were larger at room temperature than at higher temperature. It may be due to air humidity associated with the films at room temperature. The increase in conductivity with increasing temperature (above 50^0C) could be attributed to negative temperature coefficient and semiconducting nature of the Bi_2O_3 activated MnO_2 samples. The Bi_2O_3 activated films showed very high electrical resistance of the order of 10^5 Ω in air.

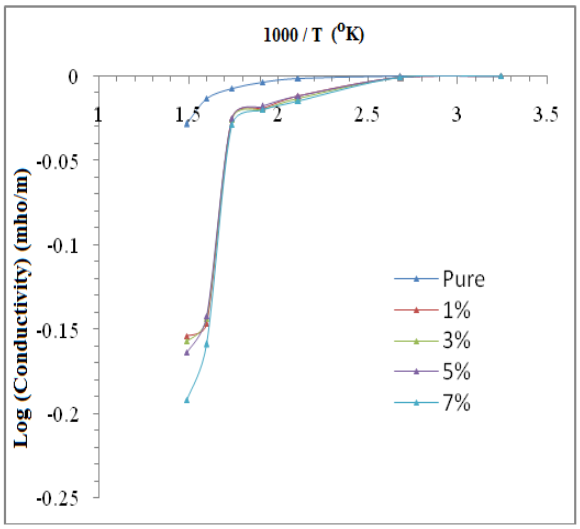

Fig. 4 Conductivity-temperature profile of Bi2O3 doped MnO2 films

From figure, it is clear that the conductivity of the sensor increases with an increase in operating temperature, indicating a negative temperature coefficient of resistance. This behavior confirmed the semiconducting nature of the undoped and doped MnO_2.

References

1. Zakrzewska, K., Thin Solid Films 391 (2) (2001) 229-238.
2. Tanaka, S., Esaka, T., J. Mater. Res. 16 (5) (2001) 1389-1395.
3. Moos, R., Int. J. Appl. Ceram. Technol. 2 (5) (2005) 345-428.
4. Kunimoto, A., Abe N., Uchida H., Katsube, T., Sens. Actuators, B 65 (2000) 122-124.
5. Kumar, M.M., Post, M. L., J. Appl. Phys. 97 (11) (2005) 114916/114911-114916/114918.
6. Schmid, W., Barsan, N., Weimar U., Sens. Actuators, B 89 (3) (2003) 232-236.
7. Espinosa AM, San José MT, Tascón ML, Vázquez MD, Sánchez Batanero P., Electrochim Acta 36 (1991) 1561.
8. D. R. Patil, L. A. Patil, Sens. Transducers 70 (2006) 661-670.
9. M. S. Wagh, G. H. Jain, D. R. Patil, S. A. Patil, L. A. Patil, Sens. Actuators B 115 (2006) 128-133.